Cement and Concrete Research 39 (2009) 446–459

Contents lists available at ScienceDirect

Cement and Concrete Research

journal homepage: http://ees.elsevier.com/CEMCON/default.asp

Release of major elements from recycled concrete aggregates and geochemical modelling

Christian J. Engelsen [a,*], Hans A. van der Sloot [b], Grethe Wibetoe [c], Gordana Petkovic [d], Erik Stoltenberg-Hansson [e], Walter Lund [c]

[a] SINTEF Building and Infrastructure, PO Box 124 Blindern, NO-0314 Oslo, Norway
[b] Energy research Centre of the Netherlands (ECN), the Netherlands
[c] University of Oslo, Norway
[d] Norwegian Roads Public Administration, Norway
[e] Norcem A.S, Norway

ARTICLE INFO

Article history:
Received 25 May 2007
Accepted 5 February 2009

Keywords:
pH
Hydrate phases
Leaching
Equilibrium
Geochemical modelling

ABSTRACT

The pH dependent leaching characteristics were assessed for different types of recycled concrete aggregates, including real construction debris and crushed fresh concrete samples prepared in laboratory. Carbonation effects were identified from the characteristic pH dependent leaching patterns for the major constituents Al, Ca, Fe, Mg, Si and SO_4^{2-}. The original particle size ranges were different for the samples investigated and this factor influenced the cement paste content in the samples which in turn controlled the leachable contents. Cement paste contents for concrete samples with fine particle size fractions (0–4 mm) were found to be higher than the originally present amount in the hardened concrete. Geochemical speciation modelling was applied over the entire pH range using the speciation and transport modelling framework ORCHESTRA, for which mineral saturation, solution speciation and sorption processes can be calculated based on equilibrium models and thermodynamic data. The simulated equilibrium concentrations by this model agreed well with the respective measured concentrations. The main differences between the fresh and aged materials were quantified, described and predicted by the ORCHESTRA. Solubility controlling mineral phase assemblages were calculated by the model as function of pH. Cement hydrate phases such as calcium silicate hydrate, calcium aluminate hydrate (AFm and AFt) and hydrogarnet were predominating at the material pH. The concentration of carboaluminates was found to be strongly dependent on the available carbonates in the samples. As the pH was decreased these phases decomposed to more soluble species or precipitates were formed including iron- and aluminium hydroxides, wairakite and amorphous silica. In the most acid region most phases dissolved, and the major elements were approaching maximum leachability, which was determined by the amount of cement paste.

© 2009 Elsevier Ltd. All rights reserved.

1. Introduction

Potential environmental impact of recycled concrete aggregate to soil and groundwater is of great concern, as the objective of most countries is to achieve high level of reuse for this material. One relevant way to judge such impact is to assess the potential release of chemical constituents from recycled concrete aggregate by leaching characterisation and subsequent geochemical modelling, in order to identify the most important release mechanisms. In order to achieve this goal, the partitioning of chemical species between the solid and the aqueous phase has to be determined on the basis of the speciation in the solution and the solid phase. One of the main controlling factors is the pH, as recognized in earlier studies [1–4]. Different surface processes can occur within the pH domain (1–14), such as ion exchange, complexation, precipitation and sorption or incorporation to a mineral phase [5–8]. In order to identify and describe the processes occurring at different pH, a thorough characterization of the leaching behaviour is first required. Characterizing the leaching behaviour over the entire pH range is important due to the strong alkaline nature of the material (e.g. cement materials), and the varying external pH encountered at the field site. Furthermore, the material pH of recycled concrete aggregate is dependent of the degree of carbonation, which obviously will vary with the service life exposure of the original concrete structure. Typical range for the material pH will thus be between the fresh concrete pH (>13) and the pH of fully carbonated material defined as the pH where the phenolphthalein colour change occurs (<10). The field site pH, however, will in many cases be in the more acid region, thus reflecting the importance of characterizing the leaching behaviour over the entire pH range.

In order to explain the main leaching mechanism(s), geochemical speciation modelling has proven to give insight to this complex matter.

* Corresponding author. Tel.: +47 22 96 55 55; fax: +47 22 69 94 38.
E-mail address: Christian.engelsen@sintef.no (C.J. Engelsen).

0008-8846/$ – see front matter © 2009 Elsevier Ltd. All rights reserved.
doi:10.1016/j.cemconres.2009.02.001

In regard to the full pH dependence characterization combined with geochemical modelling speciation of leachates from size-reduced (typical less than 4 mm) concrete aggregates derived from construction debris, some relevant studies are available [9,10]. In these studies, the pH dependent release from size reduced laboratory prepared mortars was measured. Different types of cements were used in the mortars. In addition, a modelling approach was introduced using the geochemical modelling program MINTEQA2 [11] aiming to identify solubility controlling mineral phases.

Recently, leaching processes in cement pastes have been studied by Hidalgo et al. [12] and Halim et al. [13]. In the former study the modelling code PHR QPITZ [14] including the HATCHES [15] thermodynamic database was used on the chemical composition of the leachates at pH 7 and 10. In the latter study they used PHREEQC version 2 applying a modified version of the Lawrence Livermore National Library (LLNL) database for utilisation in highly alkaline systems. In their leaching systems the leachants consisted of three different acid strengths (including one landfill eluate) ending up with final pH values of 10–12 in the leachates. Regarding solidification and stabilization of mineral waste with the use of Portland cement, different leaching and modelling approaches have been considered and a useful overview is recently given by Batchelor [2].

One challenge in regard to thermodynamic modelling of an alkaline cement leaching system is the complexity of the hydrate phases formed upon hydration i.e. C–S–H, AFt, AFm and hydrogarnet phases[1]. The hydrates are often present in mixed phases (solid solutions) where the structures and the extent of miscibility are not simple to determine [16,17]. Thus, true thermodynamic reaction constants for such mixed phases are often unknown. However, in recent studies [18,19] thermodynamic modelling was applied to calculate the pore water composition and the formation of cement hydrate phases as function of hydration time for ordinary and sulphate resistant Portland cements. In these important studies, chemical equilibrium constants were given for the main hydrate phases in the cement paste system on the basis of available data in the literature, recalculations and estimates, considering different solid solution formations.

In this paper we have focused on the pH dependent leaching characteristics of the major elements Al, Ca, Fe, Mg, Si and S. Detailed knowledge of the leaching behaviour of the major cement hydrate phases is required for identifying the release mechanisms for minor and trace elements. Four recycled concrete aggregate batches (carbonated and not carbonated) collected at commercial recycling facilities were studied. These samples were compared to a well documented concrete sample (not carbonated) prepared in laboratory with Portland cement (CEM I). In addition, cement paste content related to particle size of the concrete samples and effects of carbonation on equilibrium eluate concentrations were studied. Thus, samples with different particle size and different extent of aging were selected. Geochemical speciation modelling was applied on the leaching results over the entire pH range, using the speciation and transport modelling framework ORCHESTRA [20] in Leaching Expert System (Leach-XS) which served as the data management tool [21]. An extended version of the thermodynamic database MINTEQA2 [22] was used for the highly alkaline systems, including the latest thermodynamic modelling developments [18,19]. The main objective for the modelling work was to compare the computer modelled data with the measured leaching data in order to estimate the relevance of the geochemical modelling approach for crushed concrete leachates. The same model setup was used for constituent concentrations in leachates from well defined crushed laboratory concrete as well as leachates from real concrete aggregates (construction debris). In all cases a test focused on the pH dependence of leaching was used [23]. Previous leaching studies of soil and municipal solid waste incinerator (MSWI) bottom ash demonstrated that certain leaching processes (e.g. sorption, complexation etc.) can be adequately explained by geochemical modelling speciation using the ORCHESTRA modelling framework [6,24,25]. The present study was part of the Norwegian Road Recycling R&D program [26].

2. Materials and methods

2.1. Materials

Five different recycled concrete aggregates (RCA) batches were prepared, as shown in Table 1. Sample batch A, B and C, each of approximately 500 kg, were collected from the recycling facility BA Gjenvinning in Oslo. They originated from different old concrete and masonry buildings, i.e. they were partly carbonated. At the recycling plant the concrete and masonry rubble was crushed in a jaw crusher and the reinforcement bars were removed during this stage. Following this, the material was separated into different grain size ranges by sieving. Sample batch A was taken from a large pile that had been stocked for several years, whereas sample batches B and C were taken from the production line (at the end of the conveyer belt). Sample batch D originated from a section of the highway E6 (25 km south of Oslo) that was constructed with concrete pavement in the beginning of the 1980s. Due to reconstruction, the concrete pavement was demolished. The demolished concrete was subsequently crushed (jaw crusher) and sieved into a grain size of 20–120 mm. This material was then applied in test segments of the road base in the entrance lane to the reconstructed highway. Leaching experiments from these test fields are ongoing and they are described elsewhere [27]. Sample batch D (20–120 mm) was taken from these test fields on the day of construction. In addition, cores of the old road pavement were also taken before demolition in order to assess the carbonation level and the concrete quality in terms of compressive strength. Carbonation was insignificant as the concrete layer had been covered with asphalt.

In addition to the *real* concrete sample batches described above, sample batch E was prepared in laboratory using Portland cement (Norcem Industrisement, CEM I), natural Norstone AS aggregate (see

Table 1
List of sample batches and sample properties.

	Sample[a]						
	A	B	C	D	E1	E2	E3
Particle size (mm)[a]	0–10	10–20	10–38	20–120	0–4	4–8	8–16
Classification (Type)[b]	2	2	2	1	1	1	1
Material pH[c]	11.6	11.9	12.0	12.6	12.7	12.7	12.8
Total carbon (%)	2.51	1.56	1.78	0.37	0.32	0.25	0.21
Total inorganic carbon (%)[d]	0.92	0.88	0.88	0.13	0.060	0.039	0.027
Total organic carbon (%)	1.59	0.68	0.90	0.24	0.26	0.21	0.18
Solid Humic Acid (g/kg)	0.5	0.25	0.25	n.r.[f]	n.r.[f]	n.r.[f]	n.r.[f]
DHA fraction[e]	0.02–0.1	0.02–0.1	0.02–0.1	n.r.[f]	n.r.[f]	n.r.[f]	n.r.[f]
Selective extractions (g/kg):							
Fe-Dithionite	n.d.[g]	n.d.[g]	n.d.[g]	n.d.[g]	4.37	3.32	2.91
Fe-Ascorbate	n.d.[g]	n.d.[g]	n.d.[g]	n.d.[g]	2.96	2.30	1.85
Al-Oxalate	n.d.[g]	n.d.[g]	n.d.[g]	n.d.[g]	23.7	18.2	15.6
Leached at pH <2 (g/kg)							
Fe	2.34	3.28	1.43	2.41	4.46	3.23	2.99
Al	3.31	3.79	2.78	2.85	5.67	3.88	3.29

[a] Samples A, B, C and D was collected at a recycling plant. Samples E1–E3 were prepared in laboratory using standard Portland cement. Prior to experiments, the samples were further ground, see text.
[b] According to Norwegian declaration system [31].
[c] pH taken from the eluate of the leaching test with no addition of acid and base.
[d] Determined as total inorganic carbon (TIC) by the TOC analyser and verified by TGA-MS. For sample A, the TGA-MS values were used, see text.
[e] Dissolved Humic Acid (DHA) fraction of the leached dissolved organic carbon (DOC).
[f] Not relevant parameter.
[g] Not determined.

[1] Cement chemistry notation: C = CaO; S = SiO_2; A = Al_2O_3; m = mono; F = Fe_2O_3; t = tri; H = H_2O; $\overline{S}$ = SO_3 $\overline{C}$ = CO_2.

Table 2
Mineral phase contents (%) in samples A, D and E1 after removal of the cement paste contents with HCl analysed by XRD.

Mineral	A	D	E1
Albite, $NaAlSi_3O_8$	29.7	16.7	34.4
Actinolite, $Ca_2(Mg, Fe)_5[(OH, F): Si_4O_{11}]_2$	n.d.[a]	9.1	n.d.
Anorthite, $CaAl_2Si_2O_8$	n.d.	22.9	n.d.
Biotite, $K(Mg, Fe^{II})_3[(OH, F)_2:(Al, Fe)Si_3O_{10}]$	2.3	2.4	3.8
Chlorite, $(Mg, Al, Fe)_6[(OH)_8: (Si, Al)_4O_{10}]$	12.2	2.3	5
Cordierite, $Mg_2Al_4Si_5O_{18}$	3.6	n.d.	3.4
Diopside, $CaMg(SiO_3)_2$	n.d.	n.d.	2.7
Hematite, Fe_2O_3	1.8	n.d.	1.4[b]
Microcline, $KAlSi_3O_8$	15.9	8.0	18.4
Quartz, SiO_2	34.6	38.6	31
Total	~100	~100	~100

The quantification was carried out using Rietveld Refinement.
[a] Not detected.
[b] Maghemite, Fe_2O_3.

Table 2 for mineral composition) and admixture (super plasticizer SSP 2000). The cement contained Portland clinker (94%), gypsum (4.4%), limestone filler (<0.4%), iron sulphate (0.6%) and triethanolamin (grinding aid, 0.06%). It was cast in steel mould cubes of 100 x 100 x 100 mm. The casting volume was 45 L, forming 33 specimens. Demoulding was carried out the day after casting. The concrete mix was prepared with a water/cement ratio of 0.6, a cement content of 325 kg/m^3 and the admixture content was 1.95% of the cement weight. Fresh and hardened concrete properties were determined according to the standards EN 12350 and 12390 [28,29]. The casting, curing and hardening were carried out in the concrete laboratory of Norcem A.S. Following a hardening period of 150 days, the cubes were size reduced (laboratory jaw crusher) and fractionated (sieved) into sample batches E1, E2 and E3, with the particle size ranges 0–4 mm, 4–8 mm and 8–16 mm respectively as listed in Table 1. Total concentrations of the elements under consideration in this study are given in Table 3 for all batches. As samples E1–E3 were prepared with the same cement, the total element content was only determined in sample E1. In Table 4 the composition of the cement used for sample batch E is shown, together with its Bogue composition of cement clinker phases.

X-ray diffraction (XRD) spectrometry analyses were performed by Heidelberg Technology Center (HTC) for samples A, D and E1 before and after removal of the binder content with hydrochloric acid (HCl). All samples were dominated by quarts, feldspars (albite and microcline) and to some extent phyllosilicate (chlorite) due to the contribution from the aggregates. In addition, anorthite (feldspars) was identified in sample D. Portlandite was only identified in sample D and E1 whereas a significant calcite peak was identified in sample A. The mineralogy of sample A was in accordance to what has been reported earlier for construction and demolition waste [30]. In order to describe and quantify the mineralogy of the aggregates, the paste was removed from the rest of the samples by dissolution of the samples in HCl. The quantified mineral phases in the residues are given in Table 2 and give the mineralogy of the aggregates.

Table 3
Total element concentrations in all samples.

Element	wt.% in sample				
	A	B	C	D	E1
Al	6.0	6.3	5.9	6.2	5.2
Ca	6.6	6.7	7.1	6.3	10.3
Si	25.6	26.1	25.9	28.3	24.1
S	0.2	0.2	0.2	0.2	0.3
Fe	3.3	3.6	3.2	2.4	1.8
Mg	1.1	1.3	1.2	0.9	0.7
Na	1.8	1.9	1.8	1.9	1.9
K	2.3	2.4	2.3	2.6	2.2

Table 4
Cement composition used in samples E1–E3 analysed by X-Ray Fluorescence (XRF) given as the arithmetic mean ± 1 standard deviation, $n = 3$.

	Portland cement (wt.%)
Element	
CaO	61.5 ± 0.11
SiO_2	19.8 ± 0.07
Al_2O_3	5.02 ± 0.01
Fe_2O_3	3.29 ± 0.02
SO_3	3.87 ± 0.04
MgO	2.41 ± 0.01
K_2O	1.12 ± 0.01
Na_2O	0.39 ± 0.01
Bogue composition[a]	
C_3S	51
C_2S	18
C_3A	7.7
C_4AF	10

The average estimated Bogue composition is given for the cement clinker.
[a] Estimated values: A = Al_2O_3, C = CaO, F = Fe_2O_3, S = SiO_2.

According to the Norwegian declaration scheme for recycled concrete aggregate, RCA is classified in the two main categories; Type 1 and Type 2 [31] with different requirements for unbound and bound use. For unbound use, the materials of Type 1 are required to contain more than 94% by weight of crushed concrete and/or natural aggregates. In the type 2 category, the materials must consist of more than 90% concrete, masonry and natural aggregates. In both categories the content of recycled asphalt is limited to less than 5%. The sample batches undertaken in this study belonged to both categories as given in Table 1.

The material pH in this study refers to the equilibrium pH in the leaching suspension where no acid or base has been added (see further paragraph 2.4). In Table 1 it can be seen that the material pH for samples A, B and C were significantly lower than for samples D and E, in accordance with the origin of the sample batches described above. It also indicates that sample A was slightly more carbonated than sample B and C, whereas the material pH for sample D was found to be close to the "fresh" sample E, i.e. insignificant carbonation. The carbonation level of the samples was also verified by thermogravimetric analysis (TGA) online coupled with a mass spectrometer (MS). Significant amounts of $CaCO_3$ (or other carbonates) were only expected in samples A–C (see Section 3.4).

2.2. Preparation of laboratory and test samples

All sample batches were prepared as laboratory samples according to the standards EN 932-2 and EN 15002 [32,33]. Sample batches A, B and C were reduced to approximately 50 kg by quartering and further reduced to sub batches of 12–14 kg by the splitting procedure described in EN 932-2. From these sub batches, laboratory samples of approximately 1.3–1.5 kg were prepared using the same splitting procedure. Due to the coarse particle size, the sub batches of sample batches B and C were crushed to <16 mm in a jaw crusher prior to further mass reduction and preparation of the laboratory samples. Sample batch D was sampled as 5 × 25 kg sub batches directly from the construction site. These sub batches were crushed to <16 mm prior to preparation of the laboratory samples.

Ten concrete cubes of sample batch E were crushed after 150 days curing and hardening. This was carried out by using the compression-testing machine first, in order to break the cubes into smaller pieces, and then by applying a jaw crusher. Following this, the crushed material was separated by sieving into various particle size fractions; 0–4 mm, 4–8 mm and 8–16 mm. These sample batches were further reduced by splitting to the laboratory samples E1, E2 and E3 (1.3–1.4 kg each).

One laboratory sample from each sample batch was further size reduced to a particle size of less than 1 mm using an automatic agate mortar. For laboratory samples of relatively coarse grain size, i.e. <16

and 8–16 mm, pre-crushing with granite blocks was needed in order to have an appropriate size for the agate mortar. Each of the size reduced laboratory samples were thereafter split into series of 15–20 equal test samples (each of 80–100 g), again according to the splitting procedure in EN 932-2. The size reduction from a laboratory sample into test samples (<1 mm) was conducted prior to the leaching tests.

The preparation of laboratory samples was conducted with care in order to ensure that no fine particles were lost. Furthermore, to minimize the contamination of the samples, the sample reduction was carried out on Polyethylene (PE) foil and the splitting equipment of metal was covered with PE foil.

2.3. Acid soluble content and sample homogeneity

The homogeneity of the laboratory and test samples was controlled with respect to particle size distribution and the acid soluble content. Sieving of laboratory and test samples indicated that the crushing and splitting procedure produced representative samples. The acid soluble part was measured in all samples and assumed to represent the cement paste content. In general, this assumption is only valid for samples with acid inert aggregates. However, calculations showed (Section 3.3.3) that this assumption was reasonable for sample E1. The procedure for measuring the acid solubility is based on a modification of the standard NT Build 437 [34]. In short, the test samples were ground to <125 μm in a stainless steel Culatti MFC mill (Culatti AG, Zürich, Switzerland) and 4 g were accurately weighed into a 250 ml beaker followed by addition of 3 ml of ethanol and 150 ml of deionized water (>18.2 MΩ cm). Ten ml of concentrated nitric acid (65% m/m analytical grade) was gently added during agitation in the water suspension by a magnetic stirrer. The suspension was agitated for 30 min. Insoluble matter was then determined gravimetrically after sedimentation (>5 h), filtration and drying. From this, the acid soluble part was calculated. In this study the acid soluble part is referred to as the cement paste content.

To calculate the variations of the paste contents between laboratory samples derived from a given sample batch and within the test sample series from a given laboratory sample, the acid soluble contents of two laboratory samples (prepared from the same batch) were compared. In the first laboratory sample, where further studies were undertaken (leaching, total content determination etc.), the acid soluble contents were determined in 3–6 test samples within the same series. The other laboratory sample used for comparison was size reduced to less than 125 μm and the acid soluble part was determined in 4 replicates. This comparison procedure was carried out for all sample batches listed in Table 1.

2.4. Leaching tests

The pH dependent batch leaching test CEN/TS 14429 was used [23]. The principle of this method is to assess the pH leaching behaviour of inorganic elements in terms of equilibrium concentrations at different pH values. In order to comply with the representative mass in EN 15002 [33], test portions of approximately 60 g was used. In each leaching test a minimum of 9 similar suspensions were prepared with deionized water (>18.2 MΩ cm) in 1000 ml acid cleaned HDPE vessels. Required amounts of 1.8–3.6 M HNO_3 (Suprapur) or 1.0 M NaOH (analytical grade) were added to the suspensions in order to achieve end-pH values in regular intervals between 2 and 13.5. A suspension with no addition of acid or base was also included in all leaching tests. The approximate quantities of acid or base additions were determined in screening tests prior to the leaching tests. The final liquid to solid ratio (L/S) used was 10 ± 0.3 ml/mg and the suspensions were equilibrated for 48 h in an end-over-end roller followed by sedimentation over night. Following this, the pH and the conductivity were determined, before the suspensions were filtrated through 0.45 μm membrane filters. The pH measured in the suspension with no acid/base addition is referred to as the *material pH*, see Table 1. The filtrates were divided into two parts: the first part was untreated (non-acidified) while the second part was acidified (pH <2 with Suprapur HNO_3). The parts were kept under freezing and cooling conditions, respectively, before different chemical analysis were performed (see below).

2.5. Chemical analysis

A variety of analytical techniques were applied for chemical analysis of the eluates. Inductively coupled plasma–optical emission spectrometer using a Varian Vista ICP-OES (Varian Ltd, Australia) was used to determine major elements (Al, Ba, Ca, Fe, K, Mg, Na, S and Si), typical metal cations (Cd, Cu, Mn, Ni, Pb and Zn) and elements that under certain conditions form oxyanions (As, B, Cr, Mo, Sb, Se and V). The anions Cl^-, Br^-, SO_4^{2-} and F^- were analysed by ion chromatography (Dionex IC25, CA, US) and the dissolved organic carbon (DOC) and dissolved inorganic carbon (DIC) were measured by a total organic carbon (TOC) analyser (Shimadzu 9000a) in the eluates. Measurements of pH in the eluates were conducted on a computerized titration system (Metrohm Basic Titrino 794), while the conductivity was measured with an ion analyser (Hach Sension analyzer). The measured concentrations of all elements in the eluates were used in the geochemical model (see Section 2.6).

Sulphur and phosphorous determined by ICP-OES were assumed to be sulphate and phosphate, respectively. Sulphate is an essential species in geochemical modelling. It is also an important species in the aluminate hydrate phases in the cement paste. The sulphate results determined by the two analytical techniques were in most cases within 15% relative difference. Only at the materials pH, the relative differences were 70% and 30% for samples D and E1, respectively, most likely due to concentrations close to the limit of detection. The overall agreement was, however, considered to be fair as the released concentrations varied for more than two orders of magnitude over the pH range studied.

Chemical analyses were also conducted on the solid materials. The same elements determined in the eluates by ICP-OES were determined in the solid samples by the same technique after the materials were ground to <125 μm in the agate mortar and decomposed by a mixture of concentrated HNO_3 and $HClO_4$ (9.5 ml + 0.5 ml). Total Inorganic Carbon (TIC) contents were determined (as CO_2) by Shimadzu SSM TOC analyser by acidification with concentrated H_3PO_4. As the inorganic available carbon was important in this study, thermogravimetric analyses (TGA) were carried out for all samples using TGA7 thermogravimetric analyser (Perkin Elmer) with TAC 7/DX thermal controller (Perkin Elemer). The heating was performed in either nitrogen or oxygen atmosphere at a gradient of 5 °C/min. Sample weights of 40–80 mg pulverised (<125 μm) solid material were used. The outlet gas was analysed online using a HPR-20 quadrupole mass spectrometer (Hiden Analytical) with regard to CO_2.

The total carbon (TC) contents in all samples were determined by combustion and infrared detection (Eltra CS 800, Neuss, Germany), see Table 1. The total organic contents in the samples were estimated from the difference between TC and TIC analysis. Total element concentrations in the cement used in sample E were carried out by using X-ray fluorescence spectrometry (Philips PWW 2404).

The ICP-OES, ion chromatography, TIC and TOC (eluates) analyses were carried out at Energy Research Centre of the Netherlands (ECN). The XRF and TC determinations were conducted at Norcem A.S. All other measurements were conducted at SINTEF or University of Oslo, Department of Chemistry.

2.6. Data interpretation and geochemical modelling

The recently developed data handling and modelling software Leach-XS (Leaching Expert System) version 1.4.0.1 [21] was used. The system, which has been developed at the Energy Research Centre of the Netherlands (ECN), processes the input data needed for geochemical modelling in a systematic way. The data can be compared with existing

Table 5
Selected minerals and their formation constants (Log K).

Mineral[a]	Notation[b]	Log K	Source[c]
$Al[OH]_{3[am]}$		0.24	[18]
$Ba[SCr]O_4[77\%SO_4]$		10.13	[21]
$BaSrSO_4[50\%Ba]$		8.22	[21]
$CaCO_3$	Calcite	−8.21	[21]
$Ca(OH)_2$	Portlandite	22.80	[21]
$CaSO_4$	Anhydrite	−4.41	[18]
$CaSO_4 \cdot 2H_2O$	Gypsum	−4.60	[18]
$3CaO \cdot Al_2O_3 \cdot [Ca(OH)_2]_{0.5} \cdot (CaCO_3)_{0.5} \cdot 11.5\ H_2O$	$C_4A\bar{C}_{0.5}H_{11.5}$	−29.75	[18]
$3CaO \cdot Al_2O_3 \cdot CaCO_3 \cdot 11H_2O$	$C_4A\bar{C}H_{11}$	−31.47	[18]
$3CaO \cdot Al_2O_3 \cdot CaSO_4 \cdot 12\ H_2O$	$C_4A\bar{S}H_{12}$	−27.70	[18]
$3CaO \cdot Al_2O_3 \cdot 6H_2O$	C_3AH_6	−22.46	[18]
$4CaO \cdot Al_2O_3 \cdot 13H_2O$	C_4AH_{13}	−25.56	[18]
$CaAl_2Si_2O_8$	Anorthite		[21]
$CaAl_2Si_4O_{12} \cdot 2(H_2O)$	Wairakite	−18.87	[21]
$2CaO \cdot Al_2O_3 \cdot SiO_2 \cdot 8H_2O$	C_2ASH_8	−20.49	[21]
$Ca_6Al_2(CO_3)_3(OH)_{12} \cdot 26\ H_2O$	$C_6A\bar{C}_3H_{32}$	−41.30	[18]
$Ca_6Al_2(SO_4)_3(OH)_{12} \cdot 26\ H_2O$	$C_6A\bar{S}_3H_{32}$	−57.09	[21]
$3CaO \cdot Fe_2O_3 \cdot 6\ H_2O$	C_3FH_6	−26.78	[18]
$3CaO \cdot Fe_2O_3 \cdot CaCO_3 \cdot 11\ H_2O$	$C_4F\bar{C}H_{11}$	−35.79	[18]
$3CaO \cdot Fe_2O_3 \cdot [Ca[OH]_2]_{0.5} \cdot [CaCO_3]_{0.5} \cdot 11.5\ H_2O$	$C_4F\bar{C}_{0.5}H_{11}$	−34.07	[18]
$3CaO \cdot Fe_2O_3 \cdot CaSO_4 \cdot 12\ H_2O$	$C_4F\bar{S}H_{12}$	−32.02	[18]
$2CaO \cdot Fe_2O_3 \cdot SiO2 \cdot 8\ H_2O$	C_2FSH_8	−24.80	[18]
$[Ca(OH)_2]_{1.5}\ (SiO_2)_{0.9}\ (H_2O)_{0.9}$	Jennite	−11.85	[18]
$[Ca(OH)_2]_2\ (SiO_2)_{2.4}\ (H_2O)_2$	Tobermorite-I	−18.2	[18]
$[Ca(OH)_2]_{1.5}\ (SiO_2)_{1.8}\ (H_2O)_{1.5}$	Tobermorite-II	−13.65	[18]
$Cd(OH)_2$		−13.65	[21]
CuO	Tenorite	−7.62	[21]
$Cu(OH)_2$		−8.64	[21]
$Fe(OH)_3$	Ferrihydrite	−4.89	[21]
$Fe(OH)_{3[am]}$		5.00	[18]
$Mg_4Al_2(OH)_{14} \cdot 3H_2O$	OH-hydrotalcite	−56.02	[18]
$Mg_4Al_2(OH)_{12} \cdot CO_3 \cdot 2H_2O$	CO3-hydrotalcite	−51.14	[18]
$Mg(OH)_2$	Brucite	−16.79	[21]
MnO(OH)	Manganite	−25.27	[21]
$Ni(OH)_2$		−10.80	[21]
$PbMoO_4$		15.80	[21]
$Pb(OH)_2$		−8.15	[21]
$SiO_{2\ [am]}$	Silica	−2.713	[18]
$Zn(OH)_2$		−11.50	[21]
Zn_2SiO_4	Willemite	−15.33	[21]

[a] Only minerals that were selected with regard to the acceptable saturation indices (SI) are given. Species (e.g. HCO_3^-, OH^-, etc.) from basic aqueous reactions used in the model are not included in the table. For the relevant HFO surface complexation constants we refer to Dzombak and Morel [37].
[b] Cement chemistry and common mineral notations used in the text.
[c] Minerals from Ref. [18] that recently are included in Leach-XS thermodynamic database [21].

European regulatory criteria or leaching data from other materials in its leaching database. In addition, the system has incorporated the speciation and transport modelling framework ORCHESTRA, for which mineral saturation, solution speciation and sorption processes can be calculated based on equilibrium models and thermodynamic data [20]. In the present paper ORCHESTRA was used for geochemical speciation modelling which use an extended version of the thermodynamic database MINTEQA2 [22] for utilisation in highly alkaline systems. This extended version of the database is hereafter referred to as the Leach-XS thermodynamic database [21].

The measured leached concentrations of all elements were used as input data and the first step in the modelling procedure was to carry out a screening of the saturation levels of the mineral phases that possibly control the solubility of the elements under consideration. This is based on the calculated (by the model) ion activity product (IAP) and the given equilibrium constant (K). The saturation conditions are thus expressed as the ratio IAP/K, and in a more practical way it is expressed as the saturation index: SI = log (IAP/K). When the calculated IAP for a specific reaction is close to its corresponding K value derived from the thermodynamic database, the SI value becomes close to zero and indicates near equilibrium condition. Following the model screening, a mineral assembly is selected based on the SI values and a second geochemical speciation simulation is carried out. The mineral assembly finally used in these simulations is specified in Table 5, including the reaction equilibrium constants. From the simulations the model predicted the equilibrium concentrations and the solubility controlling phases as function of pH. Ion activity coefficients were calculated by Davies equation. Oxidizing conditions were assumed in the system and pH + pe = 15 was used in the simulations.

To include the contribution from organic matter interactions (complexation) the non-ideal competitive adsorption (NICA)-Donnan model [35,36] was integrated in the ORCHESTRA framework. In general, these interactions were not believed to be important due to the nature of the cement samples as reactive humic substances (humic and fulvic acids) are absent to a large extent. In addition, the elements under consideration in this study are available in large quantities (major species). Selective extractions of the humic substances in the samples were therefore not carried out. However, for the samples of old origin (A, B and C), where TIC and TOC were significant (see Table 1), organic matter interactions were taken into account. In the initial model calculations it was assumed that only small fractions of the solid and dissolved organic carbon determined in these samples (solid and leachates), were reactive. The fraction of reactive humic substances finally used in the model was derived from the modelling of Cu, i.e. the humic fraction was varied in the model until the differences between the predicted and measured concentrations were less than half an order of magnitude in the pH area of 4–9. The fractions were in any case small, see Table 1, but were included in the model in order to have a complete model description. For sample D and the laboratory cast samples such complexation was assumed to be irrelevant.

Specific binding of metal cations and (oxy)anions to hydrous ferric oxide (HFO) was calculated by using the generalised two-layer model of Dzombak and Morel [37]. To determine the amount of sorbent mineral applied as input in this model, selective chemical extractions were carried out for samples E1–E3. The content of amorphous and crystalline iron (hydr)oxides was determined by dithionite extraction, whereas the amorphous part was estimated by ascorbate extraction according to [38]. The aluminium (hydr)oxides in the samples were determined by oxalate extractions [39] and the results are given in Table 1. The total HFO was calculated by summing the mass of $Al(OH)_3$ and FeOOH derived from the extracted concentrations of Al and Fe respectively, and expressed as kg sorbent pr. kg dry material as required in the model. In the model amorphous aluminium hydroxide was treated as a sorbent mineral in the same way as amorphous iron oxide. This approach has been applied for soil and bottom ash materials [1,6] with promising results. The selective extractions conducted for samples E1-E3 in the present study were carried out on particles less than 1 mm (same size as in the pH dependent leaching test). For the other samples (A–D), leached concentrations of Fe and Al at pH <2 were used to calculate the HFO. The values of HFO finally used in the model are shown in Table 6 and discussed in Section 3.4.

Table 6
Calculated Hydrous Ferric Oxide (HFO) based on selective chemical extractions and leached concentrations at pH <2.

Sample	HFO (kg/kg)						
	Fe Dithionite	Fe Ascorbate	Al Oxalate	Fe pH <2	Al pH <2	Total (Fe + Al)	Total pH <2 (Fe + Al)[a]
A	n.d.[b]	n.d.[b]	n.d.[b]	0.0037	0.010	n.d.[b]	0.013
B	n.d.[b]	n.d.[b]	n.d.[b]	0.0052	0.011	n.d.[b]	0.016
C	n.d.[b]	n.d.[b]	n.d.[b]	0.0023	0.008	n.d.[b]	0.010
D	n.d.[b]	n.d.[b]	n.d.[b]	0.0038	0.008	n.d.[b]	0.012
E1	0.0070	0.0047	0.069	0.0071	0.016	0.074	0.023
E2	0.0053	0.0037	0.053	0.0051	0.011	0.057	0.016
E3	0.0046	0.0029	0.045	0.0048	0.009	0.048	0.014

[a] Values used in the model.
[b] Not determined.

3. Results and discussion

3.1. Physical properties

Compressive strength was determined for sample E in its original form. The results are shown in Fig. 1. A normal strength development for 2, 28 and 90 days was achieved, in accordance with the technical specifications given by the cement producer. An increase in compressive strength from 58 to 65 MPa was measured from 90 to 747 days. The leaching experiments were carried out after 550 days (stored in air tight containers or sealed PE bags in a climate chamber, at constant temperature and relative humidity), as also indicated in Fig. 1. It can thus be assumed that most of the cement clinker minerals were hydrated.

The compressive strengths of the concrete cores of sample D (before demolition) were 63 ± 6.4 MPa ($n = 5$). In order to account for the expected variation in the strength, all sub batches of sample D that were subject for laboratory leaching experiments, were taken at the same location after the material had been processed, fractionated and placed in the sub base of the new road. In order to roughly control the jaw crushing procedure for the laboratory concrete cubes of sample E, their sieving curves were roughly estimated (3 measuring points) after jaw crushing to <16 mm. Comparison with 4 other concrete mixes (54–82 MPa after 90 days), cast and demoulded at the same time as sample E, showed that all the mixes had approximately the same particle size distributions.

3.2. Particle size effect on paste content

In cement based material the leachability is to a large degree determined by the paste content, as most constituents will be released from this potentially soluble part of the material. When assessing leachability for samples with originally different particle sizes, it is therefore crucial to determine the paste content as this can vary due to the properties of the concrete and the crushing procedure (not necessarily seen from a sieving curve). Furthermore, the paste content can vary for samples with the same particle sizes.

In Table 7 it can be seen that the paste content (acid solubility) varied significantly. Samples E1–E3 were fractionated from the same hardened concrete mix and it was found that the paste content increased as the particle size range decreased. In addition, the paste content measured in sample E1 was found to be above the paste content originally present in the hardened concrete (before crushing) as also shown in Table 7. Thus, increased cement paste content can be expected for smaller particle size ranges due to accumulation of fine particles. This relation was also consistent with 4 other concrete mixes (not shown) pre-crushed and fractionated with the same procedure. Differences in the paste content can thus be expected at field site, when large "monolithic" concrete facilities are demolished and fractionated in different particle size ranges from the same bulk material. The paste content for sample D was in the same range as for sample E3, both coarse particle size ranges.

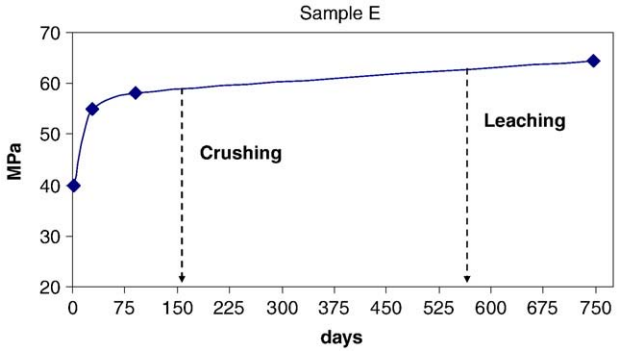

Fig. 1. Compressive strength development in sample E. Each data point is the average of two samples.

Table 7
Acid soluble contents (wt.%) in the samples with various particle size fractions[a] given as arithmetic mean ± 1 standard deviation, n = 4–6.

Sample[b]	Acid soluble part %	RSD %	Sample	Acid soluble part %	RSD %
A-1	17.2 ± 0.75	4.4	E1-1	28.4 ± 0.56	2.0
A-2	18.1 ± 0.92	5.1	E1-2	27.7 ± 0.36	1.3
B-1	13.6 ± 0.28	2.1	E2-1	18.2 ± 0.32	1.8
B-2	13.7 ± 0.49	3.6	E2-2	17.6 ± 0.70	4.0
C-1	13.6 ± 0.61	4.5	E3-1	12.6 ± 0.41	3.3
C-2	14.2 ± 0.50	3.5	E3-2	12.9 ± 1.11	8.6
D-1	12.2 ± 0.62	5.1	Concrete	19.3 ± 1.31	6.8
D-2	13.2 ± 0.63	4.8			

The acid soluble content in the Concrete sample represents the paste content in the original hardened concrete mix (sample batch E).

[a] Particle size fractions in mm: A = 0–10, B = 10–20, C = 10–38, D = 20–120, E1 = 0–4, E2 = 4–8 and E3 = 8–16.

[b] Sample codes X-1 and X-2 represent two replicate laboratory samples, mass reduced from sample batch X (i.e. A, B, C etc.).

Table 7 also illustrates the homogeneity with regard to the paste content between laboratory samples and within a test sample series (described earlier). It was found that the paste contents were not significantly different for replicate laboratory samples according to statistical analysis (95%). This proves the consistency of the splitting and mass reduction procedure.

3.3. pH dependent leaching properties

3.3.1. Acid neutralization capacity; fresh and aged materials

In general, when pH decreases in the pore water of fresh concrete, due to carbonation, the system will maintain the equilibrium by dissolution of $Ca(OH)_2$ from the cement hydrate phases which are stabilised by the high pH. This is a process that starts at the concrete surface and moves inwards, i.e. a carbonation layer will form that is growing from surface and inwards the concrete. The pore water will first be equilibrated by dissolution of portlandite ($Ca(OH)_2$) due to the chemical stability. When most of the portlandite in a commencing carbonation zone has been dissolved and precipitated as calcium carbonate, the calcium silicate hydrates (C–S–H) will release $Ca(OH)_2$, hence decalcification of C–S–H starts[2]. Monosulphate ($C_4A\overline{S}H_{12}$) and ettringite ($C_6A\overline{S}_3H_{32}$) belong to the broad groups of AFm and AFt phases respectively. The former group is more generally written $[Ca_2(Al,Fe)(OH)_6]X \cdot xH_2O$ where X denotes one formula unit of a singly charged anion or half a formula unit of a doubly charged anion (e.g. OH^-, SO_4^{2-} or CO_3^{2-} hereafter referred to as OH–AFm, SO_4–AFm and CO_3–AFm). Due to carbonation, the pH in the pore solution will eventually decrease and the X–AFm will decompose into ettringite and other aluminate compounds. At pH around 11.6, SO_4–AFm ($C_4A\overline{S}H_{12}$) and the iron containing AFm (from hydration of C_4AF) will decompose [40]. Ettringite will decompose into gypsum, calcium carbonate and aluminium hydroxide compounds, as pH is brought down to around 10.5 [40,41]. When the phenolphthalein colour change occur at pH <10 the CaO/SiO_2 ratio is approximately 0.85, and the C–S–H has been transformed into silica gel [42]. Since the carbonation starts from the concrete surface, there will be a gradient ranging from a full carbonated zone to the inner uncarbonated zone.

In order to assess the resistance to pH changes, the acid/base neutralization capacity (ANC/BNC) was determined, and the results

[2] Cement chemistry notation: C = CaO; S = SiO_2; A = Al_2O_3; m = mono; F = Fe_2O_3; t = tri; H = H_2O; $\overline{S}$ = SO_3 $\overline{C}$ = CO_2.

are shown in Fig. 2 (expressed in mmol/g). Significant differences in the materials' pH can be seen in Fig. 2, due to different degree of carbonation of the various samples. Distinct differences in the shape of the curves A–C compared with the curves D and E can be seen, as the major buffering capacities for the former curves were only found when the pH dropped below 8. This indicates the presence of calcium carbonate due to carbonation and a consequent absence of buffering cement hydrate phases. A similar situation was found in an earlier study [43] where hydrated cement mixed with different metal oxide powders was studied with imposed carbonation. The ANC capacities presented in our study are also consistent with the qualitative XRD analyses and the material pH values given in Section 2.1. These different measurements showed that sample A was slightly more carbonated than sample B and C, whereas sample D and E were insignificantly carbonated. When transferring such results to a percolation field scenario, it can be seen that sample A–C will be more sensitive to the surrounding pH (e.g. different soil infiltrates). From an environmental point of view, such material properties will consequently result in differences in the trace element release, in terms of equilibrium concentrations, compared to the non carbonated materials tested, which has been demonstrated and will be shown in a later publication. In Fig. 2b, it can also be seen that the ANC increased with increasing paste content (decreasing particle size).

3.3.2. pH dependent release

In the characterisation of the pH dependent leaching properties of cement based materials it is important to determine the release of major elements present such as Al, Ca, Fe, K, Mg, Na, S and Si. When comparing the leaching patterns of the main constituents from the aged (A–C) and the more fresh material (D and E), information regarding the presence and possible degradation of the cement hydrate phases is found. Moreover, these elements are of vital importance for the geochemical speciation modelling. In the following, sample D (in addition to E) will be referred to as "fresh" sample due to its material pH and ANC characteristics.

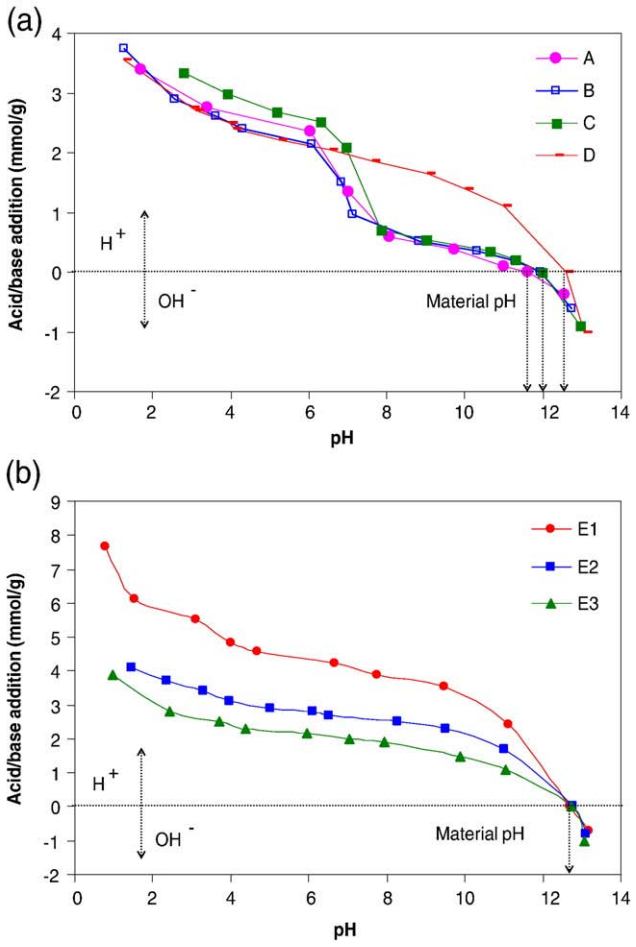

Fig. 2. Acid/base neutralisation capacities (expressed in mmol/kg) at different pH for samples (A–D) collected at field site (a) and samples (E1–E3) prepared in laboratory (b). Material pH indicates no acid/base added in the leaching test.

The pH dependent leaching of Al, Ca, Fe, Mg, S and Si is shown in Fig. 3. In general, the leaching trends for a given element were the same for the various samples. However, the leaching trends were different for the elements due to different solubility of the minerals to which the specific element is bound. From the material pH (second last alkaline data point on each leaching curve) to pH around 9, an increase in the released quantities of Ca, Mg, S and Si can be seen, whereas a decrease is observed for Al and to some extent Fe. The solubility minimum was determined for the two latter elements at slight alkaline pH. As all the hydrate phases were dissolved at this pH, the solubility of Al and Fe must be controlled by other precipitating mineral phases. In Section 3.4.2 it will be shown that wairakite ($CaAl_2Si_4O_{12}\cdot 2(H_2O)$), aluminium hydroxide and ferrihydrite could be the possible solubility controlling mineral phases around neutral pH for Al and Fe. In the most acid pH region all elements were approaching maximum leachability (available element content).

If the results in Fig. 3 are examined in more detail, distinct differences between aged and fresh material can be seen. The Al release was higher for samples A–C compared to the fresh samples D and E2 in the high alkaline region and the leaching patterns for A–C roughly followed the general solubility curve for aluminium hydroxide. Based on the presence of AFt and AFm phases at the material pH, it was reasonable to expect lower release from samples D and E2 in this pH range. The same trend can be seen from the release patterns of Fe in the high alkaline area for the aged and fresh samples. In addition, minimum release of Al and Fe was found for all samples (with some discrepancy for sample D) in the pH region of 6–9. The aging effects can also clearly be seen in the S (as sulphate) and Si release around material pH. However, the general leaching patterns for S and Si were totally different from those of Al and Fe, as expected. The S and Si release (solubility) increases at increasing carbonation level of the samples as can be seen in Fig. 3 at the material pH. This is in agreement with the fact that most of the sulphate originates from the AFt and AFm phases and the degradation of these phases will consequently be more pronounced for the aged materials (A–C) which in turn increase the sulphate solubility. For the Si-case this was in accordance with the fact that C–S–H is dissolving upon carbonation as it gradually transforms into silica gel with a different solubility. Silica gel is unstable at the high alkaline pH where the C–S–H is stable. The partly carbonated samples (A–C) consisted originally of fine particles that were fully carbonated in addition to more course particles with a carbonation layer gradient, i.e. a gradient ranging from the full carbonated zone to the uncarbonated zone inwards the particles. When the samples were ground to less than 1 mm and leaching suspensions were prepared, the material pH was determined to be 11.6–12.0 (A–C). Degradation products (e.g. partly decalcified C–S–H, silica gel etc.) originally formed in the carbonated parts of the samples were therefore exposed to this high pH and may explain why Si was more available in samples A–C at the materials pH. In addition, parts of the Si content can also be present in AFm phases, as $C_2(A,F)SH_8$ upon aging, which also changes the solubility of Si. In the pH area of 5–9, the released quantities of Si were relatively stable. In the modelling section it can be seen that these concentrations were stabilised at a concentration level close to the saturation index of amorphous silica.

The leaching patterns for Ca and Mg were also different for the aged and the fresh samples. Lower release of Ca and Mg from samples A–C compared to sample D and E2 was found at pH greater than 7. The release of Ca in particular, demonstrated the difference in the alkaline

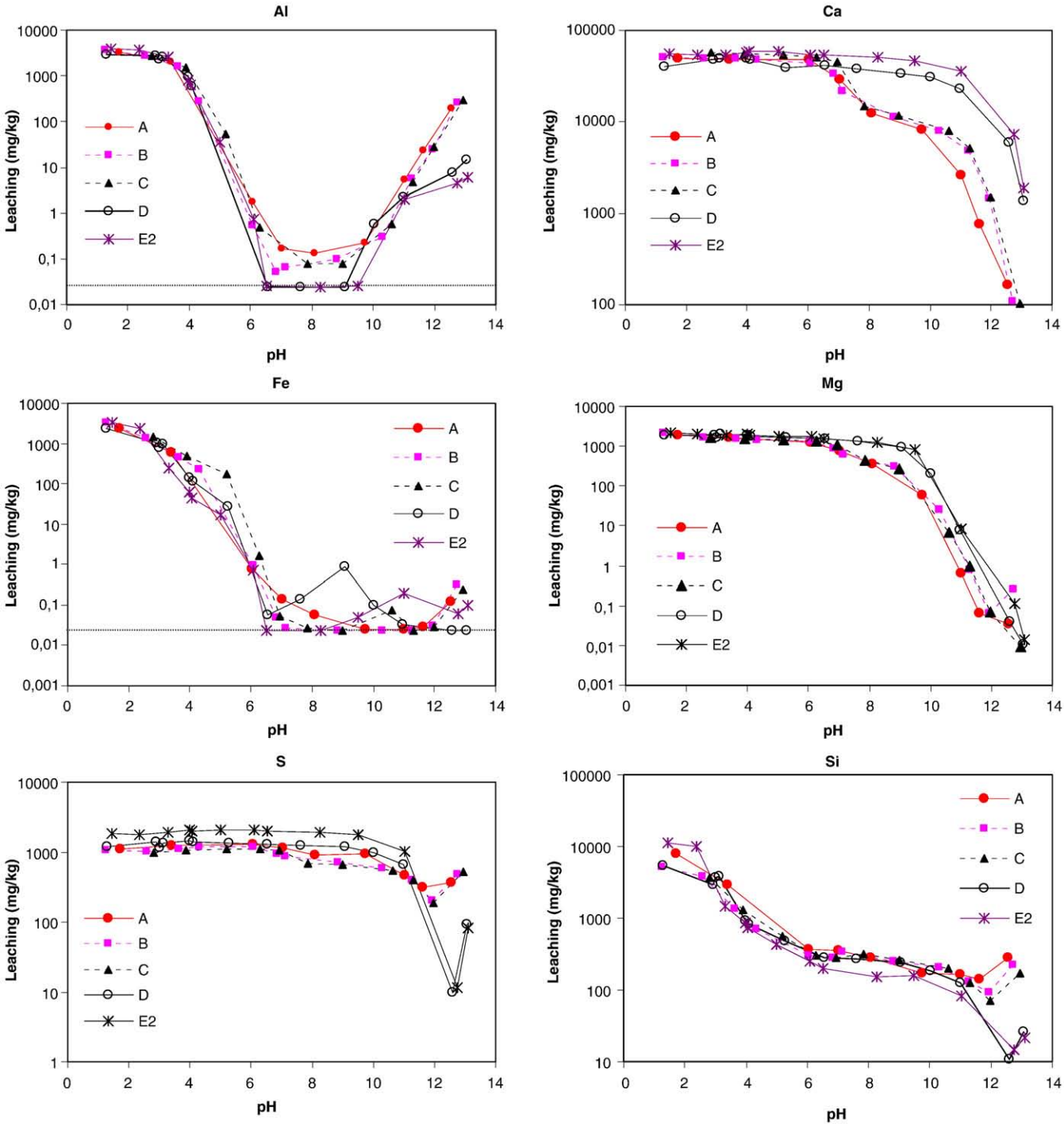

Fig. 3. pH dependent leaching of the major constituents from carbonated samples (A, B, C) and uncarbonated samples (D and E2). The second last alkaline data point in each curve show the material pH (no acid or base added). Dashed lines indicate the limit of detection of the method used for Al and Fe.

region as calcium carbonate is present due to carbonation. The relative flat plateau at pH 7–9 in Fig. 3 for samples A–C shows the calcium carbonate as a solubility controlling phase for Ca in accordance with the ANC curves in Fig. 2.

Another important trend that could be seen from the leaching pattern in Fig. 3, was the behaviour when pH was increased above the material pH. An increase in Al release was most likely due to formation of different Al (hydr)oxide complexes [44]. This influenced the stability of the sulfoaluminate hydrate phases and the sulphate release from sample E2 also increased significantly compared to sample A above material pH. For the fresh samples this can be seen as a distinct V-shape of the leaching curves in the most alkaline pH region. This trend was consistent for the other non-carbonated materials (E1 and E3), as well. With regard to the leaching patterns of Al, Ca, S and Si, we are able to distinguish between the carbonation levels of the samples in the sequence of most carbonation (A), less carbonation (B and C) and insignificant carbonation (D and E).

3.3.3. Leachability relative to the cement paste content

In the most acid region of Fig. 3, i.e. pH 1–2, the leached concentrations were at maximum as the cement pastes were degraded. The leached quantities were below the total concentrations given in

Table 3, which were determined in fully dissolved samples, i.e. acid dissolution of both paste and aggregates. In order to correlate the leachability to the cement paste content, the ratio of the leached concentrations and the total concentration in the paste (recalculated from total concentrations determined in the pure cement) was calculated as function of pH. This was carried out for sample E1, shown in Fig. 4, and gives the picture of the "paste leachability". The maximum leachabilities stabilised in the range of 95–118% of the calculated total concentration of the paste around pH 2. Considering the uncertainties in the chemical analyses (cement and leachates), preparation of the sample series in the leaching test and the acid solubility measurements, the calculations are considered to give quite accurate results.

This showed that the available contents for leaching were mainly controlled by the paste content and that there were large differences between the constituents in the same material as function of pH. The leachability of Ca and S increased from a low value at materials pH to between 70 and 80% around pH 9.5, due to decalcification of C–S–H, dissolution of portlandite and calcium sulphoaluminate hydrates (e.g. ettringite and monosulphate). The C–S–H phase starts to destabilise at higher pH than ettringite (see Section 3.3.1), which can be seen in the more rapid increase in the leachability for Ca compared to S in Fig. 4. In contrast, the leachabilities of Al and Fe were less than 0.002% at pH ~9.5.

3.4. Geochemical modelling

The modelling work was conducted mainly without any fitting of parameters. Some considerations, however, were made in regard to the calculated quantity of hydrous ferric oxide (HFO) sorption sites used in the model and the available carbonate concentrations. In general, the sorption to oxide surfaces for the major elements presented in this paper was not considered as a main leaching mechanism. However, sorption of alkaline earth cations (e.g. Ca^{2+}, Mg^{2+}) and anionic species (e.g. SO_4^{2-}, PO_4^{3-}) to reactive charged surfaces will occur at alkaline and acid pH respectively [37], and the HFO parameters in Leach-XS should thus be specified. In regard to the carbonate concentrations, the maximum determined concentrations in the eluates were measured at pH ~6, as CO_2 is released in the leachates below this pH. The pH dependent leaching results were used as input data in the computer model. Maximum element leachability from these results is used as the available quantities for reactions (not the total element concentrations). Therefore the available concentrations of carbonate used in the model, had to be separately determined in the solid phase as explained below.

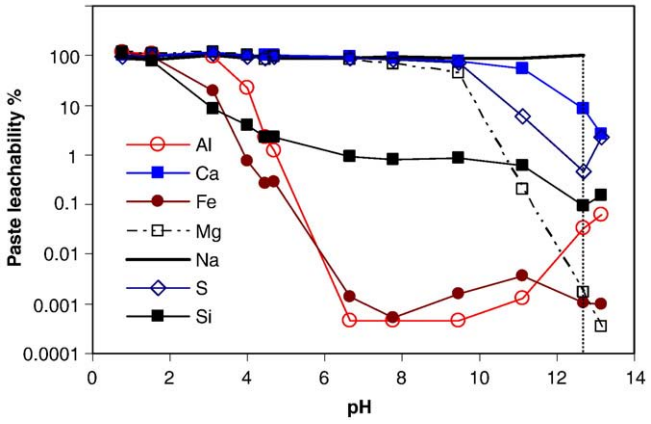

Fig. 4. The pH dependent equilibrium concentrations expressed as wt.% of the total concentrations in the paste for sample E1 as function of pH. Vertical dashed line indicates the material pH.

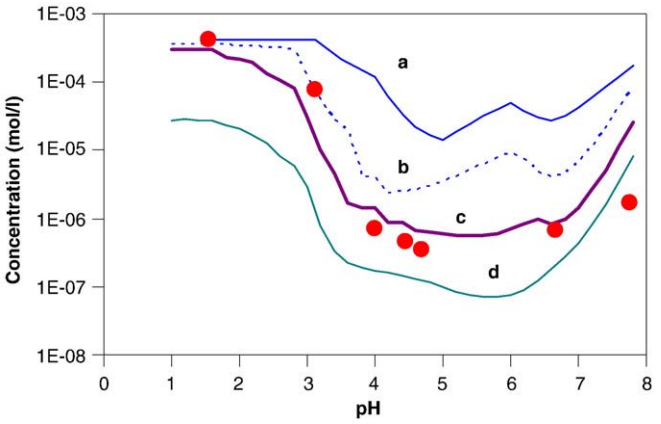

Fig. 5. Leached concentrations from sample E1 and model predictions as function of pH for PO_4^{3-}. Circle points represent the measured concentrations. Model predictions simulated with different HFO content (kg/kg); a) 0.005, b) 0.01, c) 0.026 and d) 0.07.

Hydrous Ferric Oxide (HFO) content

Based on the results in Table 1, the calculated HFO contents are given in Table 6. The contents calculated from extractions with only dithionite were virtually the same as the contents derived from the leached concentrations of Fe as can be seen in Table 6. However, the total HFO contents based on the ascorbate and oxalate extractions were 3.2–3.5 times higher than the total contents based on leached concentrations at pH <2. This was mainly caused by the Al-oxalate quantities. Assuming that anion sorption to HFO was the main leaching mechanism for PO_4^{3-} in the pH area of 4–7, the correlations between the measured and simulated concentrations are given in Fig. 5 for different HFO contents. If only sorption to amorphous iron oxide surfaces was taken into account (0.005 kg/kg) the phosphate sorption was underestimated. The most precise correlation was achieved using HFO content calculated on the basis of the leached concentrations at pH <2 (0.023 kg/kg), as sorption to HFO seemed to be overestimated when the content from the selective extractions where used (0.072). This was also the case for sample E2 and E3 (not shown), as the same correlation patterns in the same pH area were achieved for these samples as well. In addition, results from the subsequent modelling work also seemed to confirm the same HFO content in regard to sorption modelling of trace metal cations (Cu^{2+} and Ni^{2+}), using the model description in consideration. From this we can deduce that sorption to aluminium oxide surface was relevant and has to be taken into account and its inclusion to the total HFO only serves as an upper estimate. In addition, the HFO content derived from the leached concentrations proved to be in the relevant area and was therefore used for all the samples in this paper. It should also be pointed out that corrections for dissolution of HFO were conducted where it became significant. This was typically encountered at pH <4 and the corrections were made by simply subtracting the dissolved part of Al and Fe in steps of 0.5 pH units from the HFO content used in the model. By re-running the model for each step a corrected simulated leaching curve for pH <4 was achieved, and these predictions were finally combined with the original simulations and speciation calculations. The modelling curves in Fig. 5 were corrected for HFO dissolution. For the modelling of the other elements in this study such corrections were unnecessary. This was based on the observed behaviour of the other elements during the phosphate modelling.

Carbonate content

The carbonate value used in the model corresponded to the total inorganic carbon (TIC) determined in the solid samples. The results from the TGA-MS clearly showed significant amounts of carbonates (7–8% equivalent $CaCO_3$) in the samples A–C calculated from the weight loss in the temperature range of 600–800 °C. The temperature region was selected based on the MS peaks. The TGA-MS results are shown for

sample A in Fig. 6. In this figure the organic and inorganic CO_2 are recognised as the first (200–500 °C) and second (600–800 °C) MS peak, respectively. Calculations based on the weight loss of inorganic CO_2 for sample B and C agreed well with the TIC determined by the TOC analyser (see Section 2.5), while deviations were encountered for sample A. However, we emphasise that the TGA-MS analyses were carried out in triplicates (TIC only single measurement) on different test samples of sample A and showed very consistent results. Thus, the carbonate values from these determinations were used in the model for sample A. The deviation could be caused by inhomogeneity of the particular sample (due to small sample amount used for the analysis). Note that such possible error was not expected during the leaching experiments as larger sample amounts were used (~1000 times).

The TGA weight loss curves for samples D and E1–E3 are shown in Fig. 7 and they exhibit different characteristics compared with the other samples. Firstly, they show a weight loss between 400 and 440 °C due to dehydroxylation of portlandite [45,46]. We notice that portlandite was present in sample D (old sample) in line with our earlier indications. This drop in weight due to dehydration of portlandite could not be seen for sample A, while a very small tendency of weight loss (400–440 °C) was seen for sample B and C (not shown). The latter could explain the higher materials pH measured for these samples compared to sample A as they seemingly had the same carbonate contents. Furthermore, we see from Fig. 7 that the weight losses in the temperature area of 600–800 °C were small, but significant, in line with the small amount of limestone filler added to this cement. In the following, the modelling runs for samples A, D and E will be shown, as they cover carbonated and noncarbonated samples.

Contribution from the aggregate part

It was shown in Fig. 4 that the elements under consideration in this study were leached from the cement paste in sample E1 (similar calculation is difficult to carry out for real samples due to unknown formulation). However, the influence (leaching) from the aggregates can obviously not be excluded, in particular from samples taken from the recycling facility. Tossavainen and Forrsberg [47] assessed the potential leaching of major, minor and trace constituents from natural rock materials. Regarding the granite and gneiss samples, the released quantities of Ca, K and S were reported to be 1.3–5.6%, 2.1–8.7% and 8.5–10%, respectively, relative to the total concentrations in the solids. The lowest release was reported to be below 0.2% and 0.1% for Al and Si, respectively. Since they used solely pulverised rock materials (<125 μm) and performed the leaching tests at the L/S-ratio of 100 (so-called availability test), the contribution from the aggregates in our study is expected to be significantly smaller. As the model use the measured leached concentrations (suspension of both paste and aggregate), any contribution from the aggregates will be accounted for.

3.4.1. Solubility prediction

The minerals included for geochemical speciation modelling in this work are listed in Table 5, and were selected on the basis of the saturation indices (SI). In the recent study of Lothenbach and Winnefeld [18] a description of the C–S–H-, AFt-, AFm- and hydrogarnet phases and their possible formations of solid solution is given. Regarding the C–S–H phases, the solid solution approach of Kulik and Kersten [48] was used in the modelling in [18]. This included the end members $SiO_{2[am]}$ and tobermorite-I at low Ca/Si ratio whereas the end members jennite and tobermorite-II were used to describe the C–S–H at high Ca/Si ratio. The solubility products reported in [18] for the respective C–S–H phases were calculated by these authors by graphical fitting according to their measurements of Ca, Si and pH. These log K data were included in the Leach-XS thermodynamic database and used in this study, see Table 5. In general, it is challenging to model all considered elements simultaneously with one set of minerals, solid solutions and sorptive phases. Due to the complexity of the phase system and the use of generalised assumptions, such as ideal solid solutions and estimated solubility products, the model results in our study are related to uncertainties. Improvements can be made in parallel to further improvements of the underlying thermodynamic data.

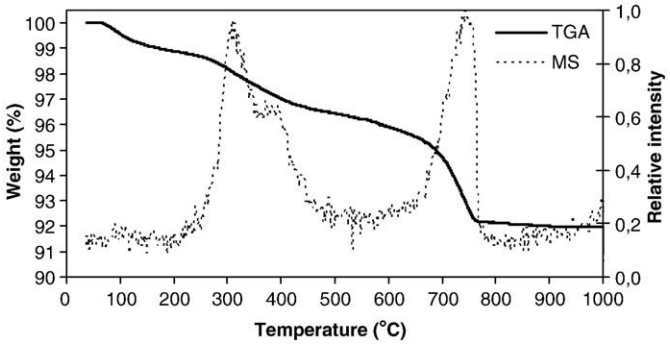

Fig. 6. Weight % (TGA) of sample A as function of temperature. Dashed curve shows the evolved CO_2 simultaneously detected with mass spectrometry (MS). Purge gas is O_2.

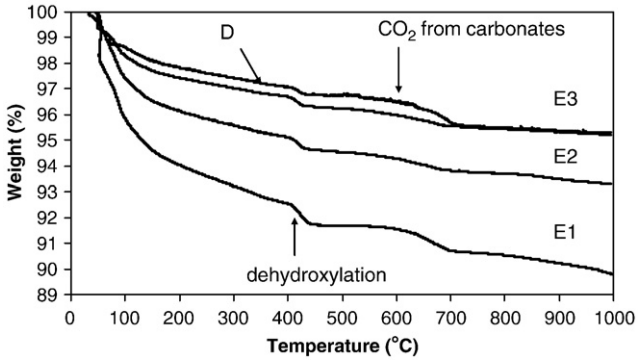

Fig. 7. Weight % (TGA) as function of temperature for samples D, E1, E2 and E3. Purge gas is N_2.

The results for Al, Ca, Mg, Si, Fe and S (as SO_4^{2-}) are shown in Fig. 8. In general, the determined pH dependent concentrations were well simulated for these elements. Uncertainties were expected to occur as the mechanistic modelling cover the whole pH range and therefore involve exhaustions of hydrate phases (congruent and incongruent), precipitation and complete dissolution of mineral phases. Furthermore, the reaction kinetics were not taken into account as the system was assumed to be near equilibrium, which is not always the case for some reactions [49]. However, the solubility shapes for most of the simulated curves matched the measured concentrations. Separate simulations showed that when only the more common mineral phases (e.g. $Al(OH)_3$, AlO(OH) etc.) were used in the modelling of Al, the solubility was strongly overestimated in the most alkaline pH area for the uncarbonated samples. This was also the case for the solubility predictions of Fe and S, when leaving out the mineral phases known to occur in the cement paste. Thus, including the reaction constants for the cement hydrate phases currently available in the database proved to give predicted values that were considerably closer to the measured concentrations.

3.4.2. Mineral phase prediction

The solubility predictions gave a characteristic picture that reflected the measured concentrations in a reasonable way for the elements under consideration. This is a sound basis for describing the controlling leaching mechanisms. In order to fully understand some of the main leaching processes in this complex chemical system the mineral and solution speciation behind the solubility predictions need to be assessed. In this study we give a geochemical speciation proposal on the basis of the thermodynamic reaction constants that are available in the extended database in Leach-XS. In Fig. 9 the distribution of

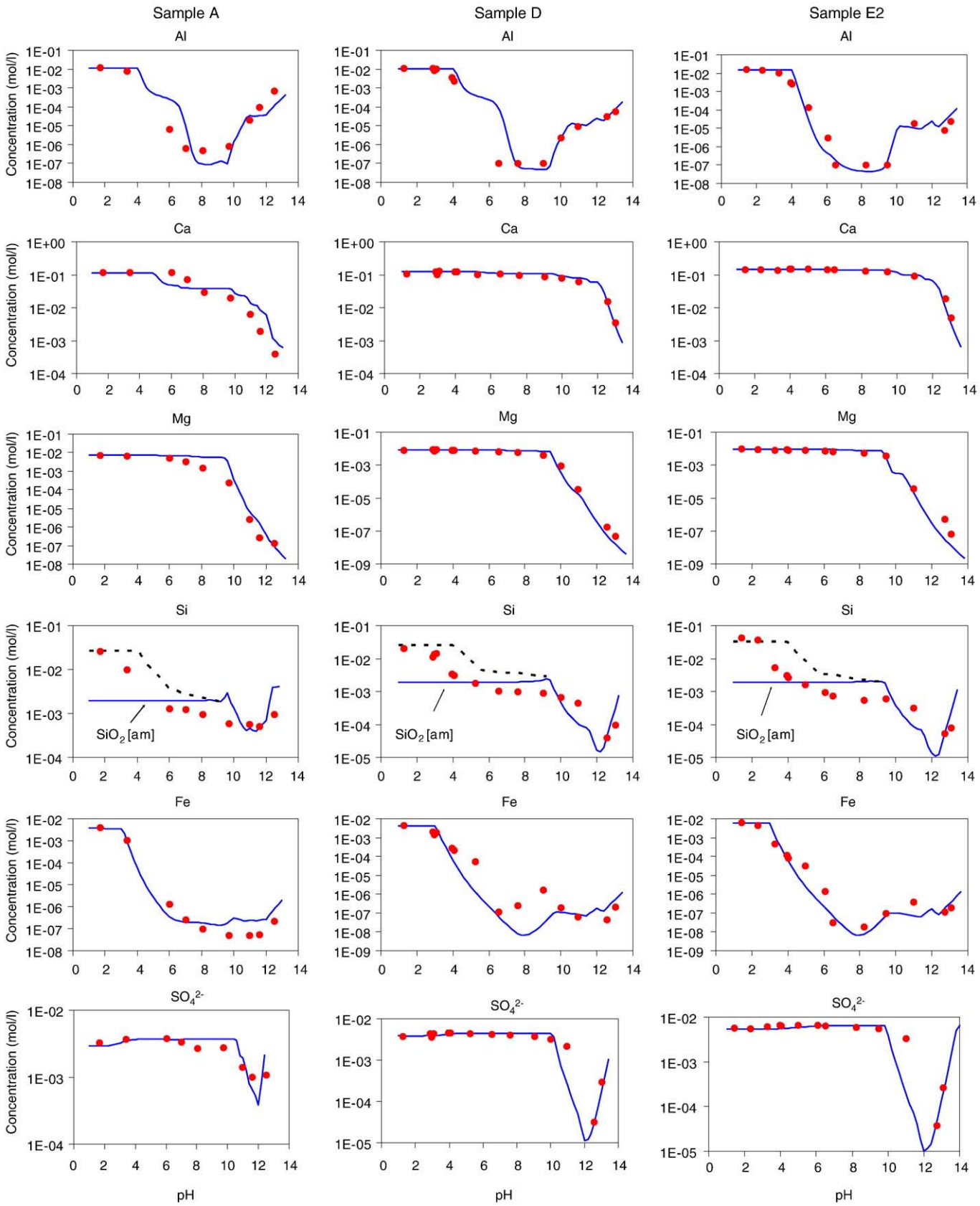

Fig. 8. Leached concentrations and model predictions as function of pH of Al, Ca, Mg, Si, Fe and SO_4. The diagrams for samples A, D and E1 are placed to the left, in the middle and to the right respectively. Circle points and lines represent the measured concentrations and the model predictions respectively. Dashed curves, show predicted values for Si solubility controlled by only wairakite.

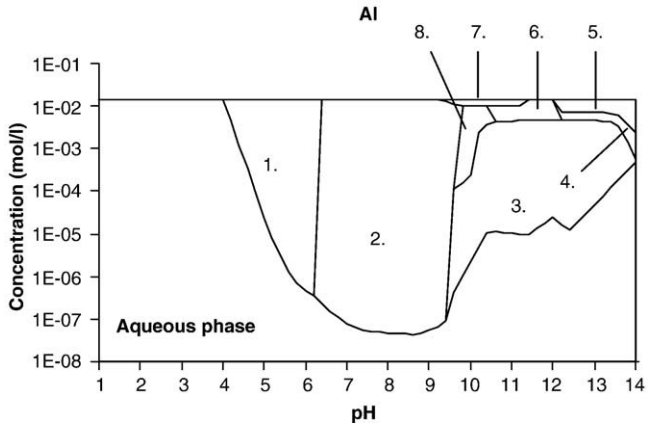

Fig. 9. Partitioning of Al^{3+} in aqueous and solid phases (1–8) as function of pH calculated by the model for sample E2. The predicted mineral phases are 1. Aluminium hydroxide ($Al(OH)_3$), 2. Wairakite [$CaAl_2Si_4O_{12}\cdot 2(H_2O)$], 3. Ettringite, 4. Hemi-carboaluminate ($C_4A\overline{C}_{0.5}H_{11.5}$), 5. Hydrogarnet ($C_3AH_6$), 6. Strätlengite ($C_2ASH_8$), 7. CO_3-hydrotalcite [$Mg_4Al_2(OH)_{12}\cdot CO_3\cdot 2H_2O$] and 8. Anorthite ($CaAl_2Si_2O_8$).

Al in solid and aqueous phases is shown as function of pH for sample E2. The specific predicted mineral phases are also given. The results from such speciation calculations for the elements under consideration are given in Tables 8 and 9 at material pH (12.7 and 11.6), pH 8, pH 6.5 and pH 4.6. The data was extracted from the speciation simulations according to the predicted concentrations in Fig. 8. For the sake of data presentation only the calculated values for sample A and E2 are reported.

Table 8
Speciation calculation of the solubility controlling mineral phases for major elements in sample E2.

Mineral	Ca	Si	Al	Fe	SO_4^{2-}	Mg
pH = 12.7						
Portlandite	29	–	–	–	–	–
Jennite	36	98	–	–	–	–
Ettringite	9.4	–	32	–	99	–
$C_4A\overline{C}_{0.5}H_{11.5}$	3.6	–	18			
$C_4F\overline{C}_{0.5}H_{11.5}$	7.9	–	–	100		
C_3AH_6	7.3	–	50	–	–	–
Brucite	–	–	–	–	–	100
HFO	1.4	1.8	–	–	–	–
Aqueous phase	5.2	0.2	0.2	–	0.9	–
pH = 8						
Calcite	1.4	–	–	–	–	–
$Silica_{[am]}$	–	1.2	–	–	–	–
Ferrihydrite	–	–	–	100	–	–
Wairakite	4.9	90	100	–	–	
HFO	0.7	2.8	–	–	–	12
Aqueous phase	93	6.1	–	–	100	88
pH = 6.5						
$Silica_{[am]}$	–	49	–	–	–	–
$Al(OH)_{3[am]}$	–	–	50	–	–	–
Ferrihydrite	–	–	–	100	–	–
Wairakite	4.9	45	50	–	–	–
HFO	–	–	–	–	1.5	–
Aqueous phase	95	6.0	–	–	99	100
pH = 4.6						
$Silica_{[am]}$	–	94	–	–	–	–
$Al(OH)_{3[am]}$	–	–	98	–	–	–
Ferrihydrite	–	–	–	100	–	–
HFO	–	–	–	–	12	–
Aqueous phase	100	6.0	2.3	0.1	88	100

It is given as the distribution of the elements among the solid and aqueous phases in the leaching suspensions at pH 4.6, pH 6.5, pH 8 and pH 12.7 (material pH). The results are given in mol% of element relative to the maximum leachable concentration.

Table 9
Speciation calculation of the solubility controlling mineral phases for major elements in sample A.

Mineral	Ca	Si	Al	Fe	SO_4^{2-}	Mg
pH = 11.6						
Calcite	60	–	–	–	–	–
Ettringite	5.7	–	20	–	*82*	–
Tobermorite-I	13	70	–	–	–	–
C_2ASH_8	7.5	17	75	–	–	–
C_2FSH_8	3.4	7.6	–	100	–	–
Brucite	–	–	–	–	–	84
CO_3-Hydrotalcite	–	–	5	–	–	16
HFO	1.5	3.7	–	–	–	–
Aqueous phase	7.5	1.8	0.3	–	18	–
pH = 8						
Calcite	60	–	–	–	–	–
$Silica_{[am]}$	–	1.1	–	–	–	–
Ferrihydrite	–	–	–	98	–	–
Wairakite	5	88	100	–	–	–
HFO	0.4	2.3	–	–	–	14
POM	0.6	–	–	2.4	–	4
Aqueous phase	34	7.5	–	–	100	82
pH = 6.5						
Calcite	59	–	–	–	–	–
$Silica_{[am]}$	–	49	–	–	–	–
$Al(OH)_{3[am]}$	–	–	49	–	–	–
Ferrihydrite	–	–	–	95	–	–
Wairakite	2.5	44	49	–	–	–
HFO	–	–	–	–	2.9	0.3
POM	0.4	–	–	4.6	–	2.7
Aqueous phase	37.5	7.4	1.2	–	97	97
pH = 4.6						
$Silica_{[am]}$	–	93	–	–	–	–
$Al(OH)_{3\ [am]}$	–	–	91	–	–	–
Ferrihydrite	–	–	–	92	–	–
HFO	–	–	–	–	0.3	–
POM[a]	–	–	0.7	7.6	–	0.6
Aqueous phase	100	7.4	8.8	0.2	100	99

It is given as the distribution of the elements among the solid and aqueous phases in the leaching suspensions at pH 4.6, pH 6.5, pH 8 and pH 11.6 (material pH). The results are given in mol% of element relative to the maximum leachable concentration.
[a] Particulate organic material.

Speciation at materials pH

At the material's natural pH the elements were distributed among the cement hydrate phases and carbonation products, as can be seen in Tables 8 and 9 for sample E2 and A, respectively. For sample E2 the model predicted portlandite, jennite and ettringite as the major solubility controlling phases (in addition to smaller contributions from AFm and hydrogarnet as will be discussed later) for Ca, Si and SO_4^{2-}. For the same elements in sample A the following phases were predicted: large content of calcite (60 mol% of Ca), tobermorite (due to the shift in pH relative to jennite), ettringite (significant lower content compared to sample E2). The latter phase may be an overestimation as the difference between A and E2 was expected to be somewhat larger based on the leaching patterns discussed earlier (Section 3.3.2). Moreover, portlandite was not predicted to control the Ca solubility for sample A, see Table 9. Thus, the model was able to predict different contributions from specific phases and different solubility controlling phase assemblages on the basis of speciation calculations, in fair agreement with the material properties (fresh and aged). Note that the predictions of C–S–H phases are idealised to the C–S–H solid solution by the end members tobermorite and jennite.

Regarding the possible AFm hydrate phases for Al and Fe at materials pH, the predictions were considered as far more uncertain, due to the lack of a complete descriptive solid solution system for the broad group of AFm phases, as pointed out by Lothenbach and Winnefeld [18]. In general the candidate phases are several and most likely mixed in solid solutions of Al and Fe. In a recent study [16] it was concluded that limited

miscibility (solid solution formation) is expected between SO_4^{-}, OH^{-} and CO_3–AFm phases and it can therefore be assumed that they behave as separate phases. From the cement characterisation in Table 4 we can see that significant quantities of the ferrite phases (C_4AF) were calculated in addition to the aluminates (C_3A) for sample E. Moreover, gypsum (4.4 wt.%) was interground in the cement used. In addition, sample E was hydrated for 550 days prior to the leaching tests. This means that a fair amount of the AFm phases should be present, mostly formed in the second stage of hydration. Monosulphate ($C_4A\overline{S}H_{12}$) was therefore expected to be present. Only minor amounts of the hexagonal phases ($C_2(A,F)H_8$ and $C_4(A,F)H_{13}$) and the thermodynamic stable hydrogarnet (C_3AH_6) are expected to be present due to the presence of sulphates upon hydration [50]. The hexagonal phases are reported in the literature to readily occur in solid solutions between the Al- and Fe-containing hydrate phases [50]. In addition, in the presence of a carbonate source (e.g. interground limestone), carboaluminates ($C_4A\overline{C}_{0.5}H_{11.5}$ and $C_4A\overline{C}H_{11}$) and it's iron containing analogues ($C_4F\overline{C}_{0.5}H_{11.5}$ and $C_4F\overline{C}H_{11}$) will be formed, and thus suppressing the formation of SO_4–AFm [18].

The model calculations for sample E2 in Table 8 show that the Al and Fe were distributed among the hydrogarnet phase, the hemi carboaluminate phase and the iron analogue ($C_4F\overline{C}_{0.5}H_{11.5}$) with respect to the available contents (Al and Fe) distributed in these phases. This was also the case for samples E1 and E3. Park and Batchelor modelled the pore water concentration and the possible solubility controlling phases by means of saturation indices in cement stabilised waste samples using SOLTEQ-B [51]. They also indicated that calcium carboaluminate controlled the solubility of Al in their model at pH slightly above 12. With regard to hydrogarnet phases, solid solution within the compositional region of C_3AH_6 and C_3FH_6 are reported to readily occur [50]. The speciation predictions for sample E showed significant solubility control by the hydrogarnet phases since the carbonate source (limestone) in sample E was small. Model trials with increased carbonate contents representing the usual limestone content in modern cement (~4% in CEM I), showed that carboaluminates ($C_4A\overline{C}H_{11}$) was the only solubility controlling AFm phase for Al, in fair agreement with the recent findings in the literature [52]. Lothenbach and Winnefeld [18] indicated by their model calculations that hydrogarnet phases were suppressed when calcite initially was present in significant amounts. In contrast, in calcite free sulphate-resisting Portland cement paste, only hydrogarnets were predicted to be formed [19]. Moreover, when the formation of hydrogarnet is excluded, Lothenbach and Winnefeld [18] found in their model trials that $C_2(A,F)SH_8$ was the main predicted precipitate among the solid solution series phases. In our system for the aged sample A, the solid phase content of Al and Fe was predicted to be exclusively present in C_2ASH_8 and C_2FSH_8, partly confirming the recent findings [18].

In regard to the distribution of Mg at materials pH, the model predicted hydrotalcite and brucite as solubility controlling phases for Mg in sample A, whereas only brucite was suggested for sample E2, again in agreement with the difference in the carbonation level of these samples.

Speciation at pH 8

The predicted solubility controlling cement hydrate phases at materials pH were dissolved at pH 8, as can be seen in Tables 8 and 9. The solubility controlling phases for Al and Si were predicted to be mainly wairakite [$CaAl_2Si_4O_{12}\cdot 2(H_2O)$], and amorphous silica to a small extent. Wairakite belongs to the zeolite group and Hidalgo et al. [12] indicated that chabazite zeolite [$CaAl_2Si_4O_{12}\cdot 6(H_2O)$] precipitated and amorphous silica was undersaturated in the same pH range. As explained in Section 3.3.1, the calcium silicate hydrates (C–S–H) decompose to silica gel upon carbonation with a C/S ratio of approximately 0.85 and only amorphous silica should be expected to control the Si solubility. The degraded C–S–H, however, is a mixed silica complex with significant amounts of CaO left [40]. This makes it rather difficult to achieve precise calculations on the Si distribution at this point. In our leaching system, the pH was decreased *artificially* (acid addition), thus creating a solution with high concentration of Ca, and wairakite (or other zeolite hydrates) could in theory precipitate. It was also shown in Fig. 8 that a close match between the measured and predicted concentrations was achieved for Al and Si at this pH. Moreover, in model trials when only wairakite was used as the solubility controlling mineral at pH below 7–8, the Si concentrations were overestimated, as shown Fig. 8. This shows that the precipitates and the degraded hydrate phases most likely are a complex mixture of amorphous silica (also partly substituted by Al) and other aluminosilicate phases that have solubility behaviour similar to zeolite minerals (e.g. wairakite and chabazite). It should be noted that the Na and K concentrations in the leachates were not affected by the pH, which excluded a major influence of the K and Na containing silicates (e.g. albite, microcline, leucite etc) that in principle could precipitate according to their saturation indices predicted by the model.

The Ca content of wairakite was predicted to be 5 mol% relative to the total available Ca amounts for samples A and E2. In sample A, calcite predominates, but still leaving a significant amount (33 mol%) of Ca in the solution. The iron content in both samples was predicted to be precipitated as ferrihydrite (hydrous ferric oxide) at pH around 8–9, which was in line with the approach for sorption to iron (hydr)oxide surfaces described in Section 3.4. In Tables 8 and 9 it can be seen that around 12–14 mol% of the available Mg content was predicted to be sorbed to HFO at pH 8 as the major content was in the aqueous phase.

Speciation at pH 6.5–4.6

The speciation of Ca, Fe, Mg and S did not change notably when the pH was decreased from pH 8 to pH 6.5. The major predicted change was precipitation of amorphous silica and aluminium hydroxide as the wairakite was starting to dissolve at pH around 6.6. In Tables 8 and 9 this is shown in the solid phase distribution of Al and Si among these phases. A further decrease to pH 4.6 showed that the available Al and Si contents were largely distributed in the $Al(OH)_{3[am]}$ and $SiO_{2[am]}$ phases, respectively. Binding to solid and dissolved organic matter was to a small extent taken into account for sample A (see Section 2.6) and the influence can be seen for Fe and Mg in the pH area of consideration. This gives a clear indication that such interactions are relevant for the aged materials, although with low organic carbon content, and would be of particular importance when describing the leaching of trace elements.

In summary the speciation calculations in Tables 8 and 9 show a distribution among the known cement hydrate phases and carbonation products for all elements at material pH. These phases (not calcite) are dissolved at pH 8 to form other mineral phases ($Al(OH)_3$, $Fe_2O_3\times H_2O$, wairakite and SiO_2[am]). At this pH the leachable contents of SO_4^{2-} and Mg^{2+} were found mostly in the aqueous phase. When pH drops to 4.6 all the calcite is dissolved. The main part of leachable Al and Si were still in the $Al(OH)_3$ and silica form, respectively. The unleached content of Fe at pH 4.6 was predicted to be present mainly as ferrihydrite. Small parts of the leachable cations in sample A were also predicted to occur in particulate organic matter (POM) complexes.

The proposed speciation calculations give a detailed insight into the possible solubility controlling phases. The largest uncertainties in these calculations most likely occur in the alkaline region. However, with the model framework used, we were able to calculate phase assemblages that described the leaching processes encountered in the laboratory test. The main differences between the fresh and aged materials were quantified, described and predicted. Hence, at the current stage it gives an overall explanation that is quite reasonable and it should also be valuable in the leaching predictions of trace elements.

4. Conclusion

When the concrete was fractionated into different particle size ranges, it was found that the cement paste contents increased with decreasing particle size. In the samples with particle sizes of 0–4 mm the cement paste content was found to be higher than the originally present quantities in the hardened concrete. For cement based aggregates the available amount of constituents for leaching is controlled by the cement

paste content, which in turn will determine the leachability. The differences in paste content directly influenced the acid neutralisation capacity and the differences play a significant role when such materials are utilized in the field in terms of the resistance to the external field pH.

The pH dependent release proved to be very consistent and gave the characteristic pH dependent shape of the leaching curves. However, significant differences in the curve shapes in the alkaline pH range were found between aged and fresh materials. The released concentrations were predicted with fair agreement over almost the entire pH range. There are uncertainties in the predictions of the solubility controlling mixed phases (solid solutions) due to the complexity of such phases and the uncertainties of the solubility constants used. However, the overall mineral speciation predictions described the main processes, including the significance of carboaluminates, ettringite and precipitation of iron and aluminium hydroxides. The model proved to be applicable to real samples collected at the recycling site. The experimental and the modelling work in this study will also be useful for describing the leaching processes of trace metals, which are relevant from an environmental impact point of view. Trace metal leaching issues are addressed in a following publication. This may provide answers to questions related to drinking water quality and soil and groundwater impact, as required by Essential Requirement 3 of the European Construction Products Directive.

Acknowledgement

This study has been supported by Norwegian Public Roads Administration, Norcem A.S, Elkem ASA Materials and BA Gjenvinning. The authors acknowledge Morten Bjerke for skilled experimental assistance.

References

[1] J.J. Dijkstra, H.A. van der Sloot, R.N.J. Comans, The leaching of major and trace elements from MSWI bottom ash as a function of pH and time, Appl. Geochem. 21(2) (2006) 335–351.
[2] B. Batchelor, Overview of waste stabilization with cement, Waste Manage. 26(7) (2006) 689–698.
[3] H.A. van der Sloot, Developments in testing for environmental impact assessment, Waste Manage. 22(7) (2002) 693–694.
[4] H.A. van der Sloot, D. Hoede, D.J.F. Cresswell, J.R. Barton, Leaching behaviour of synthetic aggregates, Waste Manage. 21(3) (2001) 221–228.
[5] I. Bonhoure, I. Baur, E. Wieland, C.A. Johnson, A.M. Scheidegger, Uptake of Se(IV/VI) oxyanions by hardened cement paste and cement minerals: an X-ray absorption spectroscopy study, Cem. Concr. Res. 36(1) (2006) 91–98.
[6] J.J. Dijkstra, J.C.L. Meeussen, R.N.J. Comans, Leaching of heavy metals from contaminated soils: an experimental and modeling study, Environ. Sci. Technol. 38(16) (2004) 4390–4395.
[7] I. Baur, C.A. Johnson, Sorption of selenite and selenate to cement minerals, Environ. Sci. Technol. 37(15) (2003) 3442–3447.
[8] F. Ziegler, C.A. Johnson, The solubility of calcium zineate (CaZn2(OH)(6)center dot 2H(2)O), Cem. Concr. Res. 31(9) (2001) 1327–1332.
[9] H.A. van der Sloot, Characterization of the leaching behaviour of concrete mortars and of cement-stabilized wastes with different waste loading for long term environmental assessment, Waste Manage. 22(2) (2002) 181–186.
[10] H.A. van der Sloot, Comparison of the characteristic leaching behavior of cements using standard (EN 196-1) cement mortar and an assessment of their long-term environmental behavior in construction products during service life and recycling, Cem. Concr. Res. 30(7) (2000) 1079–1096.
[11] A.R. Felmy, D.C. Girvin, E.A. Jenne, MINTEQA2 Computer program for Calculating Aqueous Geochemical Equilibria, U.S. Environmental Protection Agency, Athens, 1984, EPA-600/3-84-032.
[12] A. Hidalgo, S. Petit, C. Domingo, C. Alonso, C. Andrade, Microstructural characterization of leaching effects in cement pastes due to neutralisation of their alkaline nature Part I: Portland cement pastes, Cem. Concr. Res. 37(1) (2007) 63–70.
[13] C.E. Halim, S.A. Short, J.A. Scott, R. Amal, G. Low, Modelling the leaching of Pb, Cd, As, and Cr from cementitious waste using PHREEQC, J. Hazard. Mater. 125(1-3) (2005) 45–61.
[14] L.N. Plummer, D.L. Parkhurst, G.W. Fleming, S.A. Dunkle, A computer program incorporating Pitzer's equations for calculation of calculation of geochemical reactions in brines, Water Resources Investigations Report, U.S. Geological Survey, 1988, pp. 88–4153.
[15] J.E. Cross, F.T. Ewart, HATCHES a thermodynamic database and management system, Radiochim. Acta 52/53 (1991) 421–422.
[16] T. Matschei, B. Lothenbach, F.P. Glasser, The AFm phase in Portland cement, Cem. Concr. Res. 37(2) (2007) 118–130.
[17] C.S. Walker, D. Savag, M. Tyrer, K.V. Ragnarsdottir, Non-ideal solid solution aqueous solution modeling of synthetic calcium silicate hydrate, Cem. Concr. Res. 37(4) (2007) 502–511.
[18] B. Lothenbach, F. Winnefeld, Thermodynamic modelling of the hydration of Portland cement, Cem. Concr. Res. 36(2) (2006) 209–226.
[19] B. Lothenbach, E. Wieland, A thermodynamic approach to the hydration of sulphate-resisting Portland cement, Waste Manage. 26(7) (2006) 706–719.
[20] J.C.L. Meeussen, ORCHESTRA: an object-oriented framework for implementing chemical equilibrium models, Environ. Sci. Technol. 37(6) (2003) 1175–1182.
[21] www.leachxs.net.
[22] J.D. Allison, D.S. Brown, K.J. Novo-gradac, MINTEQA2/PRODEFA2, Geochemical assessment model for environmental systems: version 3.11 databases and version 3.0 user's manual, Environmental Research Laboratory, U.S. EPA, Athens, GA, 1991.
[23] CEN/TS 14429: pH dependence leaching test (initial acid/base addition), 2005.
[24] J.J. Dijkstra, A. Van Zomeren, J.C.L. Meeussen, R.N.J. Comans, Effect of accelerated aging of MSWI bottom ash on the leaching mechanisms of copper and molybdenum, Environ. Sci. Technol. 40(14) (2006) 4481–4487.
[25] H.A. van der Sloot, J.C.L. Meeussen, A. van Zomeren, D.S. Kosson, Developments in the characterisation of waste materials for environmental impact assessment purposes, J. Geochem. Explor. 88(1-3) (2006) 72–76.
[26] G. Petkovic, C.J. Engelsen, A.O. Haoya, G. Breedveld, Environmental impact from the use of recycled materials in road construction: method for decision-making in Norway, Res. Conserv. Recycl. 42(3) (2004) 249–264.
[27] C.J. Engelsen, H.A. van der Sloot, G. Petkovic, E. Stoltenberg-Hansson, G. Wibetoe, W. Lund, Constituent release predictions for recycled aggregates at field site in Norway, in: M. Ilic, J.J.J.M. Goumans, S. Miletic, J.J.M. Heynen, J. Senden (Eds.), WASCON 2006, 6th International Conference on the Environmental and Technical Implications of Construction with Alternative Materials, Belgrade, ISCOWA, 2006, pp. 293–305.
[28] EN 12350, Testing fresh concrete; part 1-7, 1999-2000.
[29] EN 12390, Testing hardened concrete; Part 1-7, 2000-2004.
[30] G. Bianchini, E. Marrocchino, R. Tassinari, C. Vaccaro, Recycling of construction and demolition waste materials: a chemical–mineralogical appraisal, Waste Manage. 25(2) (2005) 149–159.
[31] J. Karlsen, G. Petkovic, O. Lahus, A Norwegian certification scheme for Recycled Concrete Aggregates (RCA), in: T.D. Pettersen (Ed.), Sustainable Building 2002, 3rd International Conference on Sustainable Building, 2002, Oslo, Norway, Oslo: EcoBuild.
[32] EN 932-2, Tests for general properties of aggregates - Part 2: Methods for reducing laboratory samples, 1999.
[33] EN 15002, Characterization of waste - Preparation of test portions from the laboratory sample, 2006.
[34] NT Build 437, Concrete, hardened and mortar; calcium oxide and soluble silica contents, Nordtest method, 1995.
[35] C.J. Milne, D.G. Kinniburgh, W.H. Van Riemsdijk, E. Tipping, Generic NICA-Donnan model parameters for metal-ion binding by humic substances, Environ. Sci. Technol. 37(5) (2003) 958–971.
[36] D.G. Kinniburgh, W.H. van Riemsdijk, L.K. Koopal, M. Borkovec, M.F. Benedetti, M.J. Avena, Ion binding to natural organic matter: competition, heterogeneity, stoichiometry and thermodynamic consistency, Colloids Surf., A Physicochem. Eng. Asp. 151(1-2) (1999) 147–166.
[37] D.A. Dzombak, F.M.M. Morel, Surface complexation modeling, Hydrous Ferric Oxide, John Wiley & Sons, New York, 1990.
[38] J.E. Kostka, G.W. Luther, Partitioning and speciation of solid-phase iron in salt-marsh sediments, Geochim. Cosmochim. Acta 58(7) (1994) 1701–1710.
[39] L.C. Blakemore, P.L. Searle, B.K. Daly, Methods for chemical analysis of soils; sci. rep. 80, NZ soil Bureau, Lower Hutt, New Zealand, 1987.
[40] B. Lagerblad, Carbon dioxide uptake during concrete life cycle — state of the art, CBI Report 2:2005, Swedish Cement and Concrete Research Institute.
[41] I. Baur, P. Keller, D. Mavrocordatos, B. Wehrli, C.A. Johnson, Dissolution-precipitation behaviour of ettringite, monosulfate, and calcium silicate hydrate, Cem. Concr. Res. 34(2) (2004) 341–348.
[42] B. Bary, A. Sellier, Coupled moisture-carbon dioxide-calcium transfer model for carbonation of concrete, Cem. Concr. Res. 34(10) (2004) 1859–1872.
[43] A.C. Garrabrants, F. Sanchez, D.S. Kosson, Changes in constituent equilibrium leaching and pore water characteristics of a Portland cement mortar as a result of carbonation, Waste Manage. 24(1) (2004) 19–36.
[44] C.A.J. Appelo, D. Postma, Geochemistry, groundwater and pollution, 2 ed, A.A. Balkema, Leiden, Netherlands, 2005.
[45] E.T. Stepkowska, Simultaneous IR/TG study of calcium carbonate in two aged cement pastes, J. Therm. Anal. Calorim. 84(1) (2006) 175–180.
[46] W.W. Wendlandt, 3 ed, Thermal Analysis, vol. 19, John Wiley & Sons, New York: USA, 1986.
[47] M. Tossavainen, E. Forssberg, The potential leachability from natural road construction materials, Sci. Total Environ. 239 (1999) 31–47.
[48] D.A. Kulik, M. Kersten, Aqueous solubility diagrams for cementitious waste stabilization systems: II, end-member stoichiometries of ideal calcium silicate hydrate solid solution, J. Am. Ceram. Soc. 84(12) (2001) 3017–3026.
[49] H. -R. Wenk, A. Bulakh, Minerals - Their Constitution and Origin, Cambridge University Press, Cambridge, UK, 2004.
[50] P.C. Hewlett, LEA's chemistry of cement and concrete, 4 edButterworth-Heinemann, Oxford, MA; USA, 1998.
[51] J.Y. Park, B. Batchelor, General chemical equilibrium model for stabilized/solidified wastes, J. Environ. Eng.-ASCE 128(7) (2002) 653–661.
[52] T. Matschei, B. Lothenbach, F.P. Glasser, The role of calcium carbonate in cement hydration, Cem. Concr. Res. 37(4) (2007) 551–558.